Interplay of long-range and short-range Coulomb interactions in an Anderson-Mott insulator

Baćani, Mirko; Novak, Mario; Orbanić, Filip; Prša, Krunoslav; Kokanović, Ivan; Babić, Dinko

Source / Izvornik: **Physical review B: Condensed matter and materials physics, 2017, 96**

Journal article, Published version
Rad u časopisu, Objavljena verzija rada (izdavačev PDF)

https://doi.org/10.1103/PhysRevB.96.035104

Permanent link / Trajna poveznica: https://urn.nsk.hr/urn:nbn:hr:217:616958

Interplay of long-range and short-range Coulomb interactions in an Anderson-Mott insulator

Mirko Baćani,[1,2,*] Mario Novak,[1] Filip Orbanić,[1] Krunoslav Prša,[3] Ivan Kokanović,[1,4] and Dinko Babić[5]

[1]*Department of Physics, Faculty of Science, University of Zagreb, 10002 Zagreb, Croatia*

[2]*Empa, Swiss Federal Laboratories for Materials Science and Technology, 8600 Dübendorf, Switzerland*

[3]*Laboratorium für Festkörperphysik, ETH Zürich, 8093 Zürich, Switzerland*

[4]*Cavendish Laboratory, University of Cambridge, Cambridge CB3 0HE, United Kingdom*

[5]*Institute for Medical Research and Occupational Health, 10000 Zagreb, Croatia*

(Received 8 August 2016; revised manuscript received 30 January 2017; published 5 July 2017)

In this paper, we tackle the complexity of coexisting disorder and Coulomb electron-electron interactions (CEEIs) in solids by addressing a strongly disordered system with intricate CEEIs and a screening that changes both with charge carrier doping level Q and temperature T. We report on an experimental comparative study of the T dependencies of the electrical conductivity σ and magnetic susceptibility χ of polyaniline pellets doped with dodecylbenzenesulfonic acid over a wide range. This material is special within the class of doped polyaniline by exhibiting in the electronic transport a crossover between a low-T variable range hopping (VRH) and a high-T nearest-neighbor hopping (NNH) well below room temperature. Moreover, there is evidence of a soft Coulomb gap Δ_C in the disorder band, which implies the existence of a long-range CEEI. Simultaneously, there is an onsite CEEI manifested as a Hubbard gap U and originating in the electronic structure of doped polyaniline, which consists of localized electron states with dynamically varying occupancy. Therefore, our samples represent an Anderson-Mott insulator in which long-range and short-range CEEIs coexist. The main result of the study is the presence of a crossover between low- and high-T regimes not only in $\sigma(T)$ but also in $\chi(T)$, the crossover temperature T^* being essentially the same for both observables over the entire doping range. The relatively large electron localization length along the polymer chains results in U being small, between 12 and 20 meV for the high and low Q, respectively. Therefore, the thermal energy at T^* is sufficiently large to lead to an effective closing of the Hubbard gap and the consequent appearance of NNH in the electronic transport within the disorder band. Δ_C is considerably larger than U, decreasing from 190 to 30 meV as Q increases, and plays the role of an activation energy in the NNH.

DOI: 10.1103/PhysRevB.96.035104

I. INTRODUCTION

Electron localization in solids can be a consequence both of disorder [1,2] and of Coulomb electron-electron interactions (CEEIs) [3–5], the former mechanism being known as the Anderson localization and the latter as the Mott localization. It is well known that either of these phenomena can strongly influence the transport and/or magnetic properties of a material, possibly even leading to a metal-insulator transition (MIT) [5–7]. Disorder in solids corresponds to deviations from long-range periodicity and arises from the presence of impurities and/or intrinsic structural imperfections. CEEIs can be subdivided into short-range interactions between electrons on a same impurity (onsite or Hubbard interaction) and long-range interactions between electrons on different impurities [8–10]. In real materials, disorder and CEEIs often coexist, and such systems, when on the insulating side of the MIT, are referred to as Anderson-Mott insulators [10–12]. The localizing effects of disorder and of CEEIs, as well as their interplay [13–19], are of a considerable interest in the physics of strongly correlated electrons, and it is also worthwhile to remark that many of the related concepts can be extended beyond solid state physics, e.g., to the field of ultracold atoms [20–23]. The physics of Anderson-Mott insulators is such that one has to simultaneously consider the effects of disorder and of CEEIs, which may lead to various complications. Some of these complications may be overcome by applying the following general principle: at high electron densities, electrons screen the random potential due to impurities, which weakens the disorder-induced localization. However, this simplification is often not sufficient since CEEIs may also contribute to electron localization. Therefore, sometimes one has to distinguish between the effects of disorder, long-range Coulomb interactions (LIs), and short-range Coulomb interactions (SIs).

Clarifying the coexistence of disorder and CEEIs, and their interplay, remains fundamental for the understanding of many (novel) materials, which is experimentally often challenging. The disorder band of a doped semiconducting material, formed from the dopant states around the Fermi energy E_F, has for long been a benchmark for studying the combined effects of CEEIs and disorder on electrons. It has been well established [24] that, in such systems, LIs lead to the Altshuler-Aronov corrections to the density of states for single-particle excitations at E_F on the metallic side of the MIT, whereas on the insulating side, LIs lead to a soft Coulomb gap Δ_C at E_F (and hopping conductivity within the disorder band or across the band gap in which the disorder band is situated). On the other hand, SIs lead to the formation of localized magnetic moments and the Kondo effect on the metallic side, and to the Hubbard splitting of the disorder band on the insulating side of the MIT. Thus, both LIs and SIs can introduce gaps in the spectrum of single-particle excitations. Δ_C is always soft and centered at E_F, unlike the Hubbard gap U which can be either hard or soft, and is centered at E_F only in the case of the half-filling of the disorder band [8].

*mirko.bacani@empa.ch

In this paper, we tackle the complexity of coexisting disorder and CEEIs by addressing the results of systematic transport and magnetic measurements on a strongly disordered system with intricate CEEIs and a screening that changes both with Q and T. This system is polyaniline (PANI) doped with dodecylbenzenesulfonic acid (DBSA), which has been shown to display, unlike other variants of doped PANI, rich transport properties [25] that lead to a confirmation of the Fogler-Teber-Shklovskii (FTS) model [26] of the hopping transport of localized electrons in disordered networks of chain conductors. The FTS model considers the effects of Δ_C and predicts different hopping transport exponents α as a function of T and disorder level, accounting for both $\alpha < 1$ [variable range hopping (VRH)] and $\alpha = 1$ [nearest-neighbor hopping (NNH)]. In three dimensions (applicable to our samples), the VRH α can be either $\frac{1}{2}$, $\frac{2}{5}$, or $\frac{1}{4}$, with $\alpha = \frac{1}{4}$ appearing only over a small part of the T versus disorder level plane. The mentioned experimental verification [25] comprises not only VRH, commonly found in conducting polymers, but also NNH which is rather rare in this class of materials below room temperature [27]. The observed crossover between VRH and NNH at $T < 300$ K is a consequence of a quite large localization length $L_\parallel$ along the polymer chains, which results in a small U and allows for NNH to appear at relatively low T (in PANI-DBSA, U is actually an on-mer CEEI). The applicability of the FTS model to PANI-DBSA suggests the existence of another CEEI, that is, an LI parametrized via Δ_C, which is solely a consequence of the presence of disorder [28,29]. Namely, the Coulomb interaction is not screened at long wavelengths and low frequencies due to the scarcity of mobile charge in a disordered system, which is particularly pronounced at low T since the hopping transport is phonon assisted. Thus, the Coulomb interaction remains both strong and long ranged, which consequently suppresses the density of states for single-particle excitations around E_F and leads to Δ_C. Since all our samples pertain to the case of an intrinsic half-filling of the disorder band, Δ_C and U are both centered at E_F and can therefore easily leave their footprints in the behavior of electrons around E_F. Hence, our samples represent a system with disorder-induced localized electron states, in which the screening depends on Q and/or T (via the concentration of delocalized charge), and where an LI and an SI coexist. This leaves signature in the magnetic and transport properties that we probe in order to study the mentioned peculiarities of Anderson-Mott insulators.

Our samples are pressed pellets of own-made PANI-DBSA, doped over a wide range and covering a room-temperature conductivity (σ_{RT}) range of 10^{-10}–10^{3} S/m [30]. This means that we have been able to study the electron and spin dynamics of (de)localization from a virtually nonconducting to a relatively well-conducting state of the same material. We have been able to resolve Δ_C and U, in this way inferring the roles of the LI and SI in the (de)localization phenomena, which should be applicable to other Anderson-Mott insulators at least to a certain extent. While Δ_C can be estimated from $\sigma(T)$ characteristics, U is more closely related to $\chi(T)$ data. Both $\sigma(T)$ and $\chi(T)$ undergo a crossover between distinct low- and high-T regimes, and the temperature T^* of this crossover is essentially the same for the two quantities over the whole doping range. In the case of $\sigma(T)$, the low-T regime corresponds to a VRH with α being either $\frac{1}{2}$ or $\frac{2}{5}$, and the high-T regime to an NNH marked by $\alpha = 1$. In $\chi(T)$, the crossover is seen as a kink in its paramagnetic part, reflecting a sudden change in the concentrations of the Curie (localized) spins and the Pauli (delocalized) spins, one at the expense of the other. The fact that T^* is the same for both spin and charge dynamics implies that these are interrelated.

The main features of our system are a robust Δ_C and a small U, both decreasing with increasing Q but in quite different ways. Δ_C depends on Q strongly due to the screening effects, whereas U depends on Q weakly and this dependence appears only because the onsite localized electron wave function is spread over a mer [31]. By addressing the VRH-NNH crossover using our previously established method of analyzing hopping transport $\sigma(T)$ curves [32], we find that Δ_C ranges between 30 meV (350 K) at high Q to 190 meV (2200 K) at low Q. The measured $\chi(T)$ curves are analyzed within the framework of the Kamimura model [33,34] of χ for the Anderson localization in the presence of an onsite CEEI. It follows from this analysis that the thermal energy at T^* is sufficiently large to diminish the effects of the SI, removing energy restrictions for the occupancy of the localized states. This leads to an effective closing of the Hubbard gap U and the consequent appearance of NNH in the electronic transport within the disorder band. Using this picture, we estimate that U is between 12 meV (145 K) at high Q and 20 meV (230 K) at low Q. The former value of U corresponds to $L_\parallel \sim 8.5$ Å and the latter to $L_\parallel \sim 6.4$ Å, which is consistent with the lengths of one mer of doped PANI [35]. From our $\chi(T)$ data, we have also calculated both the density of localized spins and the effective density of states at E_F for delocalized spins, separately for the low- and high-T regimes, and these results support the conclusion of an enhanced delocalization of electrons when the $T^*(Q)$ boundary is crossed by heating up. Despite this enhanced delocalization, our samples remain on the insulating side of the MIT; at $T^*(Q)$, strictly speaking, they exhibit only an insulator-insulator transition between an Anderson-Mott-Hubbard insulator and an Anderson-Mott insulator.

II. EXPERIMENT

As explained in detail in Ref. [30], the PANI-DBSA powder was produced by us using a standard oxidative polymerization of aniline and a subsequent equilibrium doping of the obtained undoped PANI in aqueous solutions of different DBSA concentrations. The doping level $Q = 4q_S/q_N$, where q_S and q_N are the concentrations of sulfur and nitrogen in PANI-DBSA, respectively, was determined by combining the proton elastic backscattering spectroscopy with the particle induced x-ray emission technique. Doped samples of eight fixed values of $0.13 \leqslant Q \leqslant 3.39$ have been studied, covering σ_{RT} in the range $\sim 10^{-5}$–10^{3} S/m, whereas the $Q = 0$ material has had a barely measurable $\sigma_{RT} \sim 10^{-10}$ S/m.

In Refs. [25,30], it is discussed extensively that PANI-DBSA is a peculiar material in which the dopant content can exceed the concentration of the protonation sites (the full protonation corresponds to $Q = 2$). Since the measured x-ray diffraction patterns reveal that our PANI-DBSA is fully

amorphous for all Q [30], the exact spatial distribution of the extra dopant is not known. However, it is evident that σ continues to increase with increasing Q even for $Q > 2$, albeit much slower than for $Q \leqslant 2$. Such a behavior has been assigned to an ordering of the hopping landscape by a homogenization of the localization potential [25], and this picture has led to confirming the FTS model in which the hopping transport exponents depend on disorder level [26].

For measurements of electrical transport, polymer powder was pressed into $\sim 8 \times 5 \times 1$ mm^3 rectangular pellets under $\sim$90 MPa. Electrical contacts in the four-point configuration were made by first depositing a thin graphite layer onto the contact area and then applying a silver paste. This resulted in contact resistances that did not exceed the sample resistance irrespective of its value. For the applied currents used in our experiment (0.01–10 μA; typically 0.1 A/m^2), we confirmed the Ohmicity of the current-voltage response for each sample over the whole investigated T range. Measurements were carried out in a closed-cycle refrigerator, from the lowest achievable temperature of $\sim$10 K up to room temperature, using a constant dc bias current and a nanovoltmeter with a 10-GΩ input resistance and a maximum input signal of 12 V.

A Quantum Design SQUID magnetometer of a resolution down to 10^{-6} emu was used to measure χ in the temperature range 10–300 K. PANI-DBSA cylinders of a 5-mm height and 5 mm in diameter had been formed by pressing, mounted onto a long polyethylene straw and then placed into the magnetometer for measurements of magnetic moment by using an isothermal 6-cm scan technique [36]. No departure from linearity in magnetic moment versus magnetic field curves was found. Measured background signal from the sample holder was subtracted from raw data. DBSA is a large molecule, its diamagnetic contribution due to atomic and ionic cores being of the order of that corresponding to the PANI mer, and the paramagnetic part of χ was extracted by subtracting the Q-dependent diamagnetic contribution as discussed in detail in Ref. [30].

III. RESULTS AND DISCUSSION

The undoped form of PANI, emeraldine base (EB), is depicted in Fig. 1(a). The dots next to the nitrogen atoms represent electron lone pairs which are not involved in the covalent bonds, and it can be seen that there are no empty states for electronic transport along the polymer; the total spin of this system is zero. If EB is treated by an acid H^+A^-, where A^- is an anion, the consequent protonation transforms the quinone ring into a benzene ring; simultaneously, the imine nitrogen becomes amine nitrogen, which results in a hole (+) and an electron (•) at the protonated amine sites, as shown in Fig. 1(b) for the fully protonated PANI [37,38]. Hence, now there are empty states available for electronic transport (which in PANI-H^+A^- commonly occurs via hopping) [27]. Notably, all our samples represent the case of the half-filling of the disorder band because each doping site is intrinsically half-filled, the difference between the samples being only in the density of the doped sites. Moreover, each protonated site carries a spin $\frac{1}{2}$ and this system is not spinless. When charge hops between these states, some become empty, some singly occupied, and some doubly occupied, and these configurations are energetically

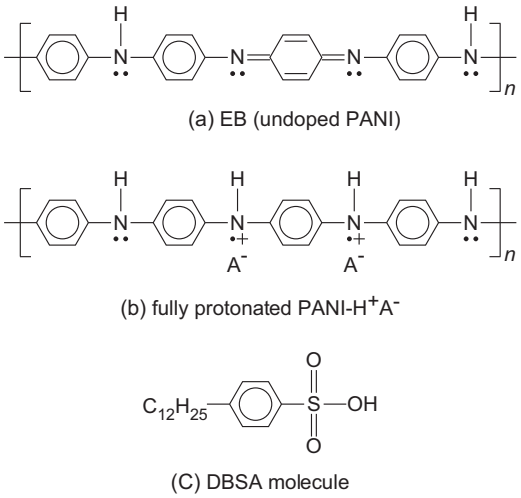

FIG. 1. (a) EB (undoped PANI). The dots represent electron lone pairs on the N atoms. (b) Fully protonated PANI-H^+A^-, obtained by a reaction of EB with an acid H^+A^-. The "+" symbols on the protonated N atoms depict holes. (c) DBSA molecule. When DBSA protonates PANI, the $C_{12}H_{25}$ tail points outwards from the PANI backbone.

different because of the onsite CEEI represented by U. Therefore, it is not unreasonable to expect that, in this structure, spin properties and charge transport might not be independent, and that this interconnection might be observable in transport and magnetic measurements. In Fig. 1(c), we show the DBSA molecule that for our samples provides A^-. This is a large molecule which protonates EB effectively while its long tail, pointing outwards, plays an important role in the entanglement of the polymer backbones [30,39]. The fact that PANI-DBSA is fully amorphous and that the electronic transport in this material is the characteristic of a hopping between localized states implies a highly disordered system subjected to the Anderson localization, in which the existence of Δ_C has been demonstrated [25]; moreover, the screening varies as a function of Q and T, and there is also a finite U. All of this makes our samples a system suitable for an experimental study of the topics outlined in Introduction.

A. Electrical conductivity and the soft Coulomb gap

Generally, the electrical conductivity of doped PANI depends on T as [27]

$$\sigma(T) = \eta_\alpha \exp[-(T_\alpha/T)^\alpha] , \quad (1)$$

which is characteristic of a hopping charge transport. For VRH, $\alpha < 1$, and for NNH, $\alpha = 1$, whereas T_α and η_α are related to energy scales and disorder at a given α [25]. At low T, one expects VRH to take place, while NNH may appear as T is increased. The most studied form of PANI, where the dopant is HCl, almost always exhibits VRH up to room temperature [32] and only fully protonated samples have been found to occasionally exhibit a crossover to NNH [40]. In contrast, PANI-DBSA undergoes this crossover well below room temperature over the whole studied doping range, as shown in detail in Ref. [25], and here we address more closely the crossover line $T^*(Q)$.

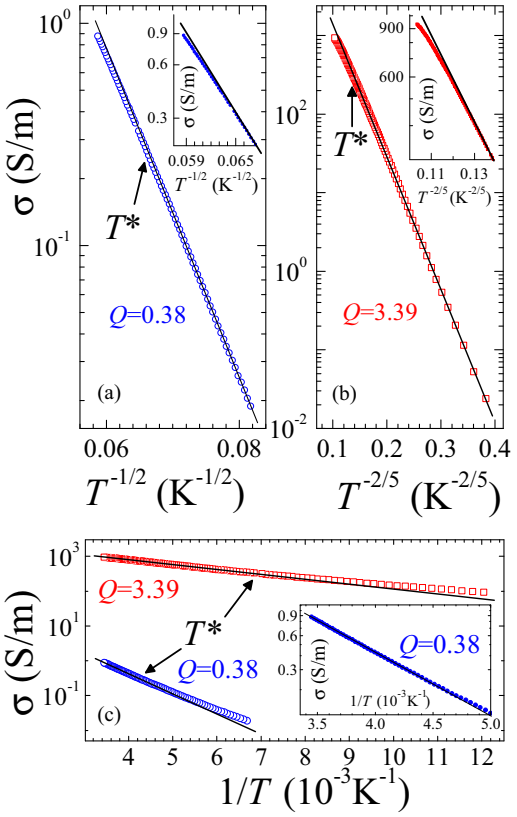

FIG. 2. (a) Experimental $\log\sigma$ vs $T^{-1/2}$ for $Q = 0.38$, exhibiting a linear behavior for T below T^* (marked by an arrow) but not when $T > T^*$. (b) $\log\sigma$ vs $T^{-2/5}$ for $Q = 3.39$ is also linear only for $T < T^*$. Insets to (a) and (b): zoom into the vicinity of T^*. (c) Plots of $\log\sigma$ vs T^{-1} for the samples from (a) and (b). These plots are linear for $T > T^*$ regardless of the low-T value of α. Inset to (c): expanded view of the linear behavior at $T > T^*$ for $Q = 0.38$. Experimental data are in all the plots shown by symbols, and the linear dependencies are outlined by solid lines.

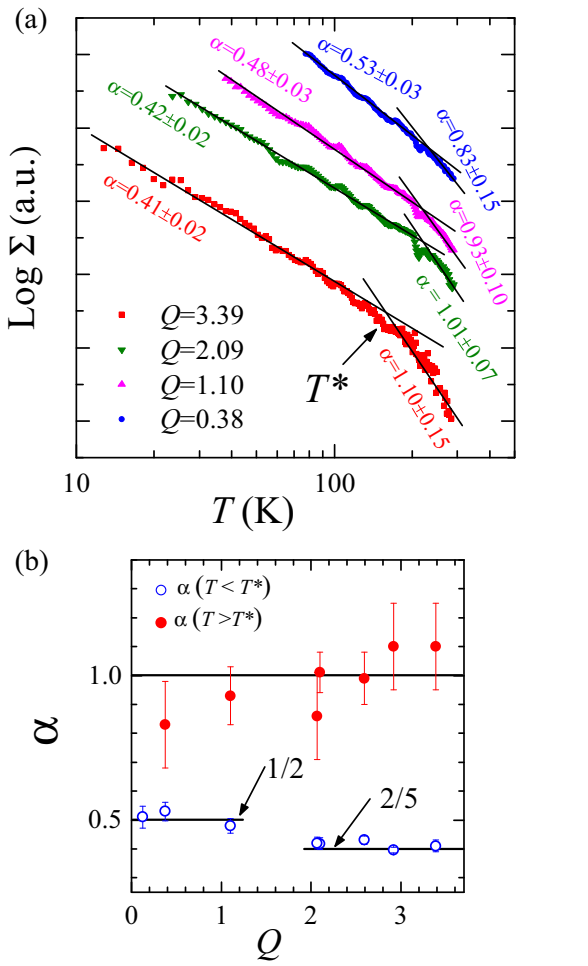

FIG. 3. (a) Experimental $\log\Sigma = \partial\ln\sigma/\partial\ln T$ vs $\log T$ for $Q = 0.38$, 1.10, 2.09, and 3.39 (symbols). At $T = T^*$, the exponent α which is given by the negative slope of the linear dependence (solid lines) [see Eq. (1)] changes from ∼0.4 or ∼0.5 (at $T < T^*$) to ∼1 (at $T > T^*$), indicating different transport mechanisms below (VRH) and above (NNH) T^*. (b) Calculated values of α (symbols) plotted against Q. Below T^*, α is close to $\frac{1}{2}$ at low Q and to $\frac{2}{5}$ at high Q. For $T > T^*$, α is close to 1 irrespective of Q.

The most straightforward way to analyze experimental data with regard to Eq. (1) is to plot them as $\log\sigma = \log e \ln\sigma$ vs $T^{-\alpha}$, where α has been chosen according to a given model prediction. If the experimental data follow the law given by Eq. (1) with a hopping exponent β that may or may not be equal to α, $\sigma(T) = \eta_\beta \exp[-(T_\beta/T)^\beta]$, there are two possibilities. The derivative

$$S = \frac{d\ln\sigma}{d\left(\frac{1}{T^\alpha}\right)} = -T_\beta^\beta \frac{\beta}{\alpha} T^{\alpha-\beta} \propto -T^{\alpha-\beta} \qquad (2)$$

is for $\beta = \alpha$ equal to $-T_\alpha^\alpha = \text{const}$ and the plot is linear. If $\beta \neq \alpha$, the plot is nonlinear, and it depends on the relation between α and β whether the experimental points will exhibit an upward or a downward curvature.

Typical $\sigma(T)$ curves of our PANI-DBSA are shown in Fig. 2 by symbols. In Fig. 2(a), the $\log\sigma$ of a low-Q curve ($Q = 0.38$) is plotted against $T^{-1/2}$ (i.e., $\alpha = \frac{1}{2}$), and in Fig. 2(b), the horizontal scale for a high-Q curve ($Q = 3.39$) is $T^{-2/5}$ (i.e., $\alpha = \frac{2}{5}$). Both these curves are linear at low T, whereas this does not hold above a certain Q-dependent T^* (shown by arrows), as seen from the mismatch of the symbols and the straight solid lines. In the insets, we zoom into the vicinity of T^* in order that the high-T departures of the experimental $\sigma(T)$ from the low-T straight lines are more clearly resolved. In both cases, $|S|$ decreases with increasing T, which according to Eq. (2) implies $\beta > \alpha$ for $T > T^*$. These $\sigma(T)$ demonstrate the general property of charge transport in PANI-DBSA: VRH at low T (with $\alpha = \frac{1}{2}$ at low Q, and $\alpha = \frac{2}{5}$ at high Q) and a more steep temperature dependence at $T > T^*$. In Fig. 2(c), we use the data from Figs. 2(a) and 2(b) to address the high-T hopping exponent by choosing the horizontal scale to be $1/T$ (hence, $\alpha = 1$ irrespective of the value of the low-T hopping exponent). It can be seen from the match of the symbols and the straight solid lines that both plots are linear for $T > T^*$ (this is for $Q = 0.38$ better seen in the inset). At $T < T^*$, the experimental points show a decrease of $|S|$ as T decreases, which according to Eq. (2) confirms that the low-T hopping exponents are smaller than unity.

The hopping exponents and crossovers between the regimes they signify can be analyzed from a different angle as well, by carrying out a derivative $\Sigma = \partial\ln\sigma/\partial\ln T$ of the data

and plotting $\log \Sigma$ against $\log T$. It follows from Eq. (1) that these plots should be linear, with a slope equal to $-\alpha$, which provides a numerical method for calculating α directly from the data. The method is demonstrated in Fig. 3(a), where we plot experimental $\log \Sigma$ against $\log T$ for $Q = 0.38, 1.10, 2.09$, and 3.39 (symbols), and fit the linear dependence (solid lines) to the data in two discernible ranges ($T < T^*$ and $T > T^*$). These results confirm the conclusions drawn on the basis of $\log\sigma$ vs $T^{-\alpha}$ plots. For $T < T^*$, the hopping exponent is $\frac{1}{2}$ for two of these Q values (0.38 and 1.10), and $\frac{2}{5}$ for the other two ($Q = 2.09$ and 3.39). For $T > T^*$, the slopes of the linear fits have larger errors due this T range being smaller, but they are for all the samples close to -1, which is again in agreement with the notion that this regime corresponds to NNH. Furthermore, the crossover temperatures are here better defined than in Fig. 2, which allows us to determine them more accurately. The values of α, calculated from $\log \Sigma$ vs $\log T$ plots for all the samples, are shown in Fig. 3(b), and the corresponding values of $T^*(Q)$ are listed in Table I.

Hence, the σ characteristics of our differently doped samples have been analyzed using three independent methods which have given consistent results. First, $\log\sigma$ vs $T^{-\alpha}$ plots have been used to deduce the low-T values of α and the upper limit of the linear behavior. Second, $\alpha = 1$ has been fixed for these plots; the linearity has been confirmed on the high-T side and the low-T limit of this behavior has been identified. Third, the hopping exponents and crossovers between them have been addressed numerically by constructing and analyzing $\log \Sigma$ against $\log T$ plots. Having these results for α and $T^*(Q)$, we now turn to the inferences of our findings.

The fact that α assumes the values of $\frac{1}{2}$, $\frac{2}{5}$, and 1 implies the existence of Δ_C in our PANI-DBSA [25] because this is at the heart of the FTS model [26]. There is a question of whether one could extract Δ_C from our $\sigma(T)$ data, similarly as this was done from crossovers between different VRH regimes (different $\alpha < 1$) for HCl-doped PANI [32]. This method is based on addressing the energy range (symmetrical around E_F) containing states involved in the hopping transport, which is given by

$$\epsilon_\alpha = \alpha k_B T \left(\frac{T_\alpha}{T}\right)^\alpha \tag{3}$$

and plays the role of an activation energy [28]. The exponents $\alpha = \frac{2}{5}$ and $\frac{1}{2}$ reflect a reduction of the density of states for charge transport, originating in the opening of a linear or quadratic soft gap, respectively, for the energies E satisfying $|E - E_F| \leqslant \Delta_C$. When ϵ_α and Δ_C are of the same order, a crossover between $\alpha = \frac{1}{2}$ or $\frac{2}{5}$ (low T) and $\alpha = \frac{1}{4}$ or $\alpha = 1$ (high T) occurs at some T^* [41]. Hence, Δ_C can be estimated from

$$\Delta_C \approx \epsilon_\gamma(T^*) = \epsilon_\delta(T^*), \tag{4}$$

where γ and δ are hopping transport exponents below and above T^*, respectively. An elegant way to account for Eq. (4) directly from the data is to use that $\epsilon_\alpha = k_B T \Sigma(T)$ regardless of α, so Eq. (4) can be written as

$$\Delta_C \approx k_B T^* \Sigma(T^*), \tag{5}$$

which can be used to read Δ_C directly from experimental curves. The results of applying Eq. (5) to the data are plotted in Fig. 4 by triangles. On the other hand, by inserting $\delta = 1$ into Eq. (4), we obtain

$$\Delta_C \approx k_B T_1, \tag{6}$$

that is, Δ_C represents the activation potential of the NNH in our samples. This finding can also be supported by qualitative arguments, as follows. If energy restrictions for the hopping between nearest neighbors are marginal (we shall address this in more detail in Sec. III B), the potential an electron has to overcome in order to hop is the (screened) Coulomb interaction with the hole left behind, and this is what underlies the concept of Δ_C in a disordered system [28,42]. In Fig. 4,

TABLE I. Parameters extracted from experimental $\chi_p(T)$ for different Q: $n(E_F)$, N_C, $k_B^{-1}\Delta N_C/\Delta n(E_F)$, and $L_\parallel = \sqrt{\hbar^2 \Delta n(E_F)/8 m_e \Delta N_C}$. Ranges of linearity in $\chi_p(T)T$ are indicated, and T^* extracted from $\sigma(T)$ is also listed.

Q	T^* from $\sigma(T)$ (K)	T range of linear $\chi_p(T)T$ (K)	$n(E_F)$ [states(eV)$^{-1}$ (2 rings)$^{-1}$]	$N_C\ 10^{-3}$ [states (2 rings)$^{-1}$]	$k_B^{-1}\Delta N_C/\Delta n(E_F)$ (K)	$L_\parallel$ (Å)
3.39	146	10–170	4.24	19.03	152	8.50
	± 5	170–300	4.93	10.00		
2.92	196	10–190	3.99	21.02	193	7.56
	± 8	190–300	4.94	5.17		
2.60	208	10–200	3.22	26.64	204	7.38
	± 5	200–300	4.15	10.27		
2.09	213	10–200	2.29	33.63	201	7.43
	± 8	200–300	3.49	12.80		
2.06	213	10–190	2.97	29.32	197	7.48
	± 8	210–300	3.84	14.54		
1.10	219	10–200	3.84	26.77	211	7.23
	± 10	210–300	5.18	2.32		
0.38	221	10–220	0.53	11.83	232	6.88
	± 15	220–300	0.83	5.81		

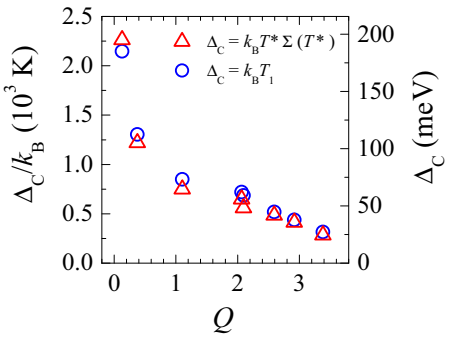

FIG. 4. Coulomb gap in PANI-DBSA, determined by two independent methods as explained in the text.

we plot by circles Δ_C extracted from the data according to Eq. (6), and these results show a good agreement with those from the application of Eq. (5). It can be seen in Fig. 4 that Δ_C decreases with increasing Q, dropping strongly from ~190 meV (2200 K) at $Q = 0.13$ to ~30 meV (350 K) at $Q = 3.38$. We believe that this appreciable decrease arises from an enhancement of the screening with increasing Q, which diminishes the disorder potential and reduces the corresponding Anderson localization.

B. Magnetic susceptibility and the onsite Coulomb interaction

The above analysis of $\sigma(T)$ provides valuable information but still leaves certain questions unanswered. While the decrease of Δ_C as Q grows implicates an enhancement of the screening and a consequent weakening of the disorder-induced localization, the reason for the crossover between VRH and NNH remains unclear when only these data are considered. In particular, an important part of the energy restrictions for the hopping between the localized states (which can be empty, singly or doubly occupied) is expected to originate in the onsite CEEI given by U (which opens a Hubbard gap). Since differently occupied sites carry different spin (0 or $\frac{1}{2}$), a natural way to approach this matter is to measure χ and compare these results to those for σ.

Measured $\chi(T)$ curves for different Q are shown in Fig. 5, where they are plotted as χT vs T (mole is defined per two rings, see Fig. 1). These plots are approximately linear, which implies [43–46]

$$\chi(T) = \frac{C_1}{T} + C_2 \,, \tag{7}$$

where C_1 and C_2 are independent of T. The first term on the right-hand side of Eq. (7) is the Curie susceptibility corresponding to localized spins at singly occupied protonation sites (see Fig. 1). The second term, C_2, comprises not only a strong diamagnetic component originating in atomic and ionic cores, but also a Pauli-type paramagnetic contribution of delocalized spins that hop from one localized state to another. Some of the curves exhibit cusps at temperatures of about 50 K, which is of little relevance for the current topic and has been discussed elsewhere [47,48]. When the diamagnetic contribution, which is of no importance for the behavior of localized and delocalized spins, is subtracted as explained in Ref. [30], one obtains the paramagnetic part χ_p of χ, as

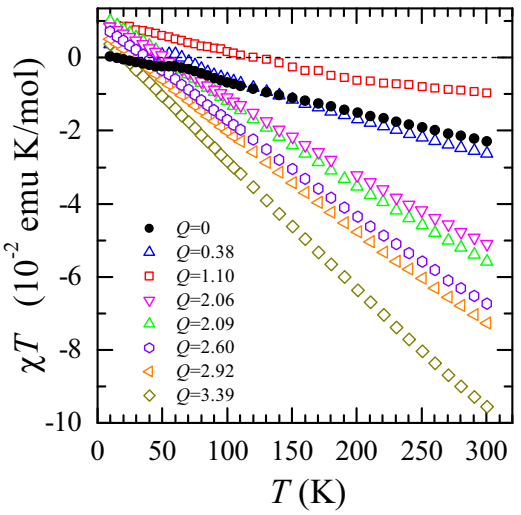

FIG. 5. χT vs T for different Q. Note that the intercept for the $Q = 0$ sample (black solid circles) is zero, i.e., there is no paramagnetism originating in localized spins.

we exemplify in Fig. 6 by plotting these data (symbols) for $Q = 0.38$, 1.10, 2.09, and 3.39. A closer inspection of these plots reveals that there are actually two ranges of linearity in $\chi_p T$ (indicated by the solid fit lines), with a crossover represented by a kink at a certain Q-dependent temperature T^* (marked by arrows). In Fig. 7, we plot this crossover temperature against Q by squares, and compare it to $T^*(Q)$ of

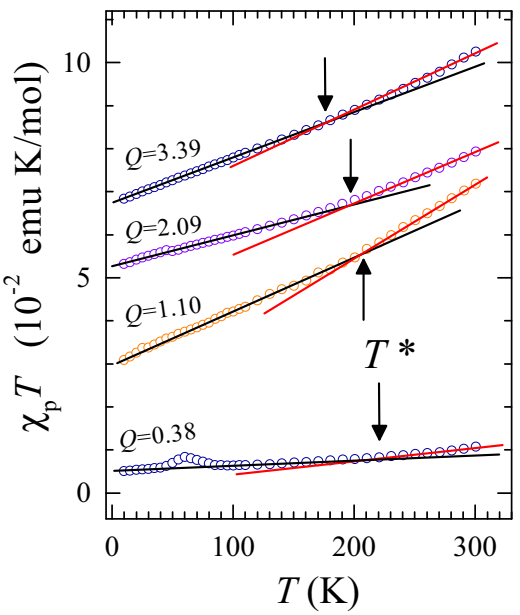

FIG. 6. Experimental $\chi_p T$ vs T (symbols) for $Q = 0.38$ and 1.10 (where $\alpha = \frac{1}{2}$ in VRH), and $Q = 2.09$ and 3.39 (where $\alpha = \frac{2}{5}$ in VRH). For clarity, the $Q > 0.38$ plots are offset vertically (each by 2 emuK/mol from the previous one). The arrows point to the positions of the crossover temperatures T^*, whereas the straight lines represent fits in the ranges of linearity. The cusp at $T \sim 50$ K for $Q = 0.38$ is of little relevance for the current topic and has been addressed elsewhere [47,48]. The physical parameters determining the linear fits are discussed in the text and listed in Table I.

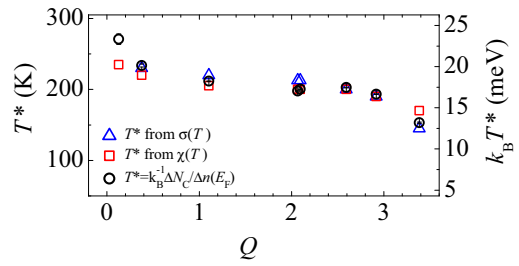

FIG. 7. Crossover temperature T^* as a function of Q, determined by three independent methods as explained in the text. Error bars are of the order of the symbol size.

the crossover between VRH and NNH, extracted from $\sigma(T)$ (triangles). Evidently, there is a good agreement between the crossover temperatures in $\sigma(T)$ and $\chi(T)$ over the whole Q range, which suggests the same underlying physics and justifies the use of the same symbol T^*. The circles represent T^* obtained by a third method, which is discussed later. A similar behavior was found for two HCl-doped PANI samples close to the full protonation [40], but these data were insufficient for establishing a more detailed physical picture. Less pronounced kinks in $\chi_p T$ vs T plots were also found for HCl-doped PANI at crossovers between different VRH mechanisms (i.e., different $\alpha < 1$), and the same mechanism, discussed below, underlies these crossovers as well (although they are less sharp than the crossover between VRH and NNH) [48].

From the plots demonstrated in Fig. 6, we can extract, separately for $T < T^*$ and $T > T^*$, several parameters which are useful in the subsequent discussion. Since the paramagnetic contribution of delocalized electrons is of a Pauli type, the slope C_2 is equal to $\mu_B^2 n(E_F)$, where μ_B is the Bohr magneton and $n(E_F)$ is an effective density of states of delocalized electrons around E_F. The intercept C_1 is equal to $N_C \mu_B^2/k_B$ because it corresponds to the Curie paramagnetism of localized spins $\frac{1}{2}$ (the concentration of which is N_C). In Table I, we list the calculated values of $n(E_F)$ and N_C for all Q. Other calculated quantities in Table I are $k_B^{-1}\Delta N_C/\Delta n(E_F)$ [where $\Delta n(E_F) = n(E_F; T > T^*) - n(E_F; T < T^*)$, and $\Delta N_C = N_C(T < T^*) - N_C(T > T^*)$], and the longitudinal localization length $L_\parallel$ (along the polymer chains).

One can note in Table I that there are two distinct regimes in $n(E_F)$: one for $Q \leqslant 1.10$ (where $\alpha = \frac{1}{2}$ in the VRH), and one for $Q > 1.10$ (where $\alpha = \frac{2}{5}$ in the VRH). In each of these regimes, $n(E_F)$ increases with increasing Q but $n(E_F)$ is for $Q = 1.10$ larger than that for $Q \approx 2$ although the conductivity is in the former case lower. However, we recall that these regimes differ in the structure of the Coulomb gap which is, as a function of energy, in the former case quadratic and in the latter case linear. This presumably affects the behavior of electrons close to E_F, which calls for a further modeling that is out of the main focus of this paper. On the other hand, the process at T^*, which is accounted for by $\Delta n(E_F)$ and ΔN_C, is insensitive to this difference, as follows. When the values of $k_B^{-1}\Delta N_C/\Delta n(E_F)$ from Table I are plotted on Fig. 7 (circles), it becomes clear that this quantity actually represents the same T^* obtained directly from the $\sigma(T)$ and $\chi_p(T)T$ curves. This leads to a conclusion that the thermal energy $k_B T^*$ plays a decisive role in the (de)localization of spins at the crossover between VRH and NNH. As T crosses T^* by heating up, Curie (localized) spins become delocalized, turning into Pauli spins, and the opposite happens in cooling down. Hence, N_C decreases (increases) by ΔN_C, whereas $n(E_F)$ simultaneously increases (decreases) by $\Delta n(E_F)$, the energy scale for this process being $k_B T^*$. For this to occur, the differences between electron energies associated with the occupancy of a localized state must be important for $T < T^*$ and marginal for $T > T^*$. We believe that a viable explanation for that can be found within the framework of the Kamimura model of χ_p for a system with the Anderson localization and onsite CEEI, which has been experimentally verified in a number of cases for doped semiconductors [33,34] and also applied to treat the coexistence of Curie-type and Pauli-type contributions in conducting disordered PANI with weak CEEIs [33,34]. In this model [33],

$$\chi_p = \frac{2\mu_B^2}{k_B T} \sum_j \left[2 + \exp\left(\frac{E_F - E_j - U_j}{k_B T} \right) + \exp\left(-\frac{E_F - E_j}{k_B T} \right) \right]^{-1} . \quad (8)$$

A hop of an electron to a singly occupied localized state costs an energy U; this sets restrictions in the sense that hopping to nearest neighbors is not necessarily the most favorable and the charge transport is consequently VRH. Simultaneously, the leading term in Eq. (8) is $\chi = N_S \mu_B^2/k_B T$, where N_S is the number of singly occupied states. This holds for any relation between U and the width W of the impurity band. When $W > U$ and T increases, the Curie contribution is suppressed and a Pauli-type behavior strengthens, becoming dominant at $T \sim U/k_B$. At $k_B T \gg U, W$, when electrons become nondegenerate (hot), a Curie-type $\chi_p(T)$ reappears but with a replacement of N_S by the total number of electrons; this regime is obviously not reached in our experiment.

In this picture, our samples are in the regime of $W > U$, and the crossover between the VRH and NNH occurs at $T^* \sim U/k_B$. The fulfillment of this criterion implies that $k_B T^*$ is large enough to diminish the energy restrictions for the hopping between differently occupied sites, which effectively closes the Hubbard gap and, in turn, sets NNH as the most efficient charge transfer mechanism. It can be seen in Fig. 7 that T^*, and consequently U, exhibits a weak decrease with increasing Q. If U were an on-atom SI, it should not depend on Q at all, but we recall that U is an on-mer SI, corresponding to more extended electron wave functions the tails of which overlap. This overlap is larger for less separated doped sites, i.e., larger Q, which increases the localization length and reduces U.

In order to test further the above picture of the effective closing of the Hubbard gap due to heating up, we have calculated the longitudinal localization length for the Anderson localization, given by [49,50]

$$L_{\parallel} \approx \sqrt{\frac{\hbar^2}{8 m_e U}}\,, \tag{9}$$

where m_e is the free-electron mass and U is in our calculation replaced by experimentally determined $k_B T^*$. As can be seen in Table I, the calculated $L_{\parallel}$ ranges from ~6.4 Å to ~8.5 Å (slightly increasing with increasing Q), which agrees well with the PANI mer size [35]. If we could estimate the localization length $L_{\perp}$ perpendicular to the polymer backbone, we would be able to calculate the localization volume $V_{loc} = L_{\perp}^2 L_{\parallel}$. We find it reasonable to assume that $L_{\perp} \sim 1$–2 Å, which is the width of the polymer backbone. This implies a relatively large V_{loc} which is by a factor of $L_{\parallel}/L_{\perp} \sim 5$ larger than that typical of a localization on a single atom. An implication of this assessment is that thermal activation within disorder band in doped PANI gives rise to a relatively high σ because $T_{\alpha} \propto 1/V_{loc}$ [5].

IV. CONCLUSIONS

Polyaniline (PANI) doped with dodecylbenzenesulfonic acid (DBSA) shares many properties with other variants of doped (electrically conducting) PANI, such as a protonation mechanism which leads to the injection of conducting charge and a relatively high conductivity, a strongly disordered structure of entangled polymer chains that results in the Anderson localization, an electrical transport via charge hopping from one localized state to another, etc. On the other hand, PANI-DBSA exhibits a behavior which is seldom found not only in doped PANI, but also in conducting polymers generally: it undergoes a crossover from a low-T variable range hopping (VRH) to a high-T nearest-neighbor hopping (NNH) below room temperature and over a wide doping range. This property was useful in an experimental confirmation [25] of the Fogler-Teber-Shklovskii model [26] of hopping transport in three-dimensional networks of chain conductors, implying the presence of a long-range Coulomb interaction that opens a soft Coulomb gap Δ_C within the impurity band. However, PANI-DBSA is a system with a short-range, onsite Coulomb interaction U as well, which generally may lead to the Mott localization. Namely, the protonation of PANI leads to singly occupied localized states, each carrying a spin $\frac{1}{2}$, which may also become empty or doubly occupied as the charge hops, and in this process, the onsite Coulomb repulsion cannot be disregarded. Having the above in mind, we here address the coexistence of long- and short-range Coulomb interactions in Anderson-Mott insulators.

Our investigation is based on comparative measurements and analysis of the T dependencies of the electrical conductivity σ and magnetic susceptibility χ of own-made PANI-DBSA pellets. The doping range of our samples covers room-temperature conductivity between 10^{-10} and 10^{3} S/m, i.e., we have tackled the physics outlined above from a virtually nonconducting to a relatively well-conducting state of a same material. The shapes of $\sigma(T)$ and $\chi(T)$ are characteristic of doped PANI, that is, $\sigma(T)$ contains a signature of a thermally activated hopping transport, whereas the paramagnetic part of $\chi(T)$ is a sum of a $1/T$ Curie-type and a T-independent Pauli-type contribution. By analyzing the $\chi(T)$ curves, we have found that they also exhibit a crossover from a low-T to a high-T regime, and that the crossover temperature T^* is, over the whole doping range, the same as that of the VRH-NNH crossover in $\sigma(T)$. Using the Kamimura model for the $\chi(T)$ of a system with the Anderson localization and a finite U, we conclude that the VRH-NNH crossover at T^* occurs because the thermal energy $k_B T^*$ is of the order of the energy differences between differently occupied localized states. Hence, in this picture, $U \sim k_B T^*$. Using this assumption, we calculate the longitudinal electron localization length $L_{\parallel}$ and obtain that it is basically equal to the PANI-DBSA mer size. This result is consistent with the structure of PANI-DBSA polymer chains and explains why U is much smaller than in the case of localized states on single atoms. In addition to $L_{\parallel}$, we determine several other parameters of importance, these being Δ_C, the effective density of states of delocalized electrons around the Fermi energy, and the density of localized Curie spins.

We find that Δ_C is robust but strongly doping dependent, ranging from 30 meV (350 K) to 190 meV (2200 K) at the highest and lowest doping, respectively, and it plays the role of the activation energy in the NNH. The strong reduction of Δ_C by doping is attributed to an enhancement of the screening of the long-range Coulomb interaction as the density of delocalized charge grows. In contrast, U is much smaller and decreases with increasing doping from 20 meV (230 K) to 12 meV (145 K). For an on-atom electron-electron interaction, U would be independent of doping, but U is here an on-mer interaction and its doping dependence is a consequence of a larger overlapping of the localized electron wave functions when these are less separated.

A small Hubbard gap U that is situated within a larger Coulomb gap Δ_C is the main feature of our system, and these two gaps govern the spin and charge dynamics in PANI-DBSA. The property of having a gap within a gap appears in many different systems, e.g., underdoped cuprate superconductors, Bechgaard salts with spin-density-wave order, etc., where a small gap or pseudogap is usually within a large hard Hubbard gap [51,52]. In our system, in contrast, the Hubbard gap is the smaller one of the two coexisting gaps. Yet, such an attenuation of the Hubbard gap (which is in our system due to an on-mer localization) is not surprising when relevant electron wave functions are spread over several sites/atoms. Because U is small, Δ_C represents the dominant energy scale in PANI-DBSA since the screening of the long-range Coulomb interaction is only partial due to the presence of disorder in the system.

ACKNOWLEDGMENTS

Discussions with L. Forró, S. Teber, I. Kupčić, and B. Batlogg are gratefully acknowledged. This work has been supported by Croatian Science Foundation under the Project No. 6216.

[1] P. W. Anderson, Phys. Rev. **109**, 1492 (1958).
[2] A. Lagendijk, B. van Tiggelen, and D. S. Wiersma, Phys. Today **62**(8), 24 (2009).
[3] N. F. Mott, Proc. Phys. Soc. London, Sect. A **62**, 416 (1949).
[4] J. Hubbard, Proc. R. Soc. London, Ser. A **276**, 238 (1963).
[5] N. F. Mott, *Metal-Insulator Transitions*, 2nd ed. (Taylor & Francis, London, 1990).
[6] P. A. Lee and T. V. Ramakrishnan, Rev. Mod. Phys. **57**, 287 (1985).
[7] M. Imada, A. Fujimori, and Y. Tokura, Rev. Mod. Phys. **70**, 1039 (1998).
[8] J. H. Davies, J. Phys. C: Solid State Phys. **17**, 3031 (1984).
[9] H. von Löhneysen, Ann. Phys. (Berlin) **523**, 599 (2011).
[10] *Conductor-Insulator Quantum Phase Transitions*, edited by V. Dobrosavljević, N. Trivedi, and J. M. Valles, Jr. (Oxford University Press, Oxford, 2012).
[11] S. Teber, Eur. Phys. J. B **49**, 289 (2006).
[12] D. Belitz and T. R. Kirkpatrick, Rev. Mod. Phys. **66**, 261 (1994).
[13] A. Richardella, P. Roushan, S. Mack, B. Zhou, D. A. Huse, D. D. Awschalom, and A. Yazdani, Science **327**, 665 (2010).
[14] E. Prati, M. Hori, F. Guagliardo, G. Ferrari, and T. Shinada, Nat. Nanotechnol. **7**, 443 (2012).
[15] K. Byczuk, W. Hofstetter, and D. Vollhardt, Int. J. Mod. Phys. B **24**, 1727 (2010).
[16] D. M. Basko, I. L. Aleiner, and B. L. Altshuler, Ann. Phys. (NY) **321**, 1126 (2006).
[17] I. S. Burmistrov, I. V. Gornyi, and A. D. Mirlin, Phys. Rev. Lett. **108**, 017002 (2012).
[18] G. Tzamalis, N. A. Zaidi, C. C. Homes, and A. P. Monkman, Phys. Rev. B **66**, 085202 (2002).
[19] M. Schreiber, S. S. Hodgman, P. Bordia, H. P. Lüschen, M. H. Fischer, R. Vosk, E. Altman, U. Schneider, and I. Bloch, Science **349**, 842 (2015).
[20] A. Aspect and M. Inguscio, Phys. Today **62**(8), 30 (2009).
[21] G. Roati, C. D'Errico, L. Fallani, M. Fattori, C. Fort, M. Zaccanti, G. Modugno, M. Modugno, and M. Inguscio, Nature (London) **453**, 895 (2008).
[22] M. Lewenstein, A. Sanpera, V. Ahufinger, B. Damski, A. Sen(De), and U. Sen, Adv. Phys. **56**, 243 (2007).
[23] B. Deissler, M. Zaccanti, G. Roati, C. D'Errico, M. Fattori, M. Modugno, G. Modugno, and M. Inguscio, Nat. Phys. **6**, 354 (2010).
[24] H. von Löhneysen, Disorder, electron-electron interactions and the metal-insulator transition in heavily doped Si:P, in *Advances in Solid State Physics 40*, edited by B. Kramer (Springer, Berlin, 2000), pp. 143–167.
[25] M. Baćani, M. Novak, I. Kokanović, and D. Babić, Synth. Met. **172**, 28 (2013).
[26] M. M. Fogler, S. Teber, and B. I. Shklovskii, Phys. Rev. B **69**, 035413 (2004).
[27] R. Menon, C. O. Yoon, D. Moses, and A. J. Heeger, Metal-insulator transition in doped conducting polymers, in *Handbook of Conducting Polymers*, edited by T. A. Skotheim, R. L. Elsenbaumer, and J. R. Reynolds, 2nd ed. (Marcel Dekker, New York, 1998), pp. 27–84.
[28] B. I. Shklovskii and A. L. Efros, *Electronic Properties of Doped Semiconductors* (Springer, Berlin, 1984).
[29] A. L. Efros and B. I. Shklovskii, J. Phys. C: Solid State Phys. **8**, L49 (1975).
[30] M. Baćani, D. Babić, M. Novak, I. Kokanović, and S. Fazinić, Synth. Met. **159**, 2584 (2009).
[31] S. Stafström, J. L. Brédas, A. J. Epstein, H. S. Woo, D. B. Tanner, W. S. Huang, and A. G. MacDiarmid, Phys. Rev. Lett. **59**, 1464 (1987), and references therein.
[32] M. Novak, I. Kokanović, D. Babić, M. Baćani, and A. Tonejc, Synth. Met. **159**, 649 (2009).
[33] H. Kamimura, Electron-electron interactions in the Anderson-localised regime near the metal-insulator transition, in *Electron-Electron Interactions in Disordered Systems*, edited by A. L. Efros and M. Polak (North Holland, Amsterdam, 1985), pp. 555–617.
[34] H. Kamimura and H. Aoki, *The Physics of Interacting Electrons in Disordered Systems* (Clarendon, Oxford, 1990).
[35] J. P. Pouget, M. E. Jozefowicz, A. J. Epstein, X. Tang, and A. G. MacDiarmid, Macromolecules **24**, 779 (1991).
[36] M. McElfresh, *Fundamentals of Magnetism and Magnetic Measurements - Featuring Quantum Design's Magnetic Property Measurement System* (Quantum Design, San Diego, 1994).
[37] A. G. MacDiarmid, J.-C. Chiang, A. F. Richter, and A. J. Epstein, Synth. Met. **18**, 285 (1987).
[38] A. G. MacDiarmid, Rev. Mod. Phys. **73**, 701 (2001).
[39] Additionally, DBSA is a surfactant leading to technologically important solubility in common solvents such as chloroform, which is rare within the whole class of doped PANI.
[40] M. Novak, I. Kokanović, D. Babić, and M. Baćani, J. Non-Cryst. Solids **356**, 1725 (2010).
[41] $\alpha = \frac{1}{4}$ has been in our PANI-DBSA observed only for the highest doping of $Q = 3.39$ (and in a rather narrow T range of $\sim$35K below the eventual appearance of $\alpha = 1$) (see Ref. [25] for details). This peculiarity has a marginal effect on the results for Δ_C presented in Fig. 4.
[42] A. L. Efros, B. Skinner, and B. I. Shklovskii, Phys. Rev. B **84**, 064204 (2011).
[43] V. I. Krinichnyi, Appl. Phys. Rev. **1**, 021305 (2014).
[44] P. Phillips, Phys. Rev. B **49**, 4303 (1994).
[45] N. S. Sariciftci, A. J. Heeger, and Y. Cao, Phys. Rev. B **49**, 5988 (1994).
[46] D. Chaudhuri, A. Kumar, R. Nirmala, D. D. Sarma, M. García-Hernández, L. S. Sharath Chandra, and V. Ganesan, Phys. Rev. B **73**, 075205 (2006).
[47] M. Baćani, Ph.D. thesis, University of Zagreb, 2014.
[48] M. Novak, I. Kokanović, M. Baćani, and D. Babić, Eur. Phys. J. B **83**, 57 (2011).
[49] N. J. Pinto, P. K. Kahol, B. J. McCormick, N. S. Dalal, and H. Wan, Phys. Rev. B **49**, 13983 (1994).
[50] N. F. Mott and E. A. Davis, *Electronic Processes in Non-Crystalline Materials*, 2nd ed. (Clarendon, Oxford, 1979).
[51] *Handbook of High-Temperature Superconductivity*, edited by J. R. Schrieffer and J. S. Brooks (Springer, New York, 2007).
[52] M. Dressel, A. Schwartz, G. Grüner, and L. Degiorgi, Phys. Rev. Lett. **77**, 398 (1996).